ADVANCED FUNCTIONAL MATERIALS
www.afm-journal.de

# Two-Step Targeted Hybrid Nanoconstructs Increase Brain Penetration and Efficacy of the Therapeutic Antibody Trastuzumab against Brain Metastasis of HER2-Positive Breast Cancer

*Chunsheng He, Jason Li, Ping Cai, Taksim Ahmed, Jeffrey T. Henderson, Warren D. Foltz, Reina Bendayan, Andrew Michael Rauth, and Xiao Yu Wu**

**Therapeutic antibodies (e.g., trastuzumab, TRA) against human epidermal growth factor receptor 2 (HER2)-positive breast cancers have shown benefits in controlling primary tumors, yet are ineffective against brain metastases due to their inability to cross the blood-brain barrier (BBB). A novel hybrid nanoconstruct system is designed to deliver trastuzumab to brain metastasis of HER2-positive breast cancer via a two-step sequential targeting approach. Self-assembly of a polysorbate 80 (PS 80)-containing polymer, lipid, and polymer-conjugated TRA forms hybrid nanoconstructs (TRA–terpolymer nanoparticles (TPN)) with high encapsulation efficiency and bioactivity. The PS 80 moiety enables the first-step targeting and receptor-mediated trancytosis across BBB is demonstrated in vitro with a 3D human BBB model in healthy and brain tumor-bearing mice. The subsequent partial dissociation of the nanoconstructs exposes the encapsulated TRA for the second-step targeting to HER2-positive cancer cells in the brain. Intravenously injected TRA–TPN delivers 50-fold TRA compared to free TRA to the brain metastasis of HER2-positive breast cancer. Treatment with TRA–TPN increases tumor cell apoptosis by 4-fold, inhibits tumor growth by 43-fold, and prolongs median survival by >1.3-fold compared to free TRA, without causing noticeable organ toxicity. These findings suggest the two-step targeted nanoconstruct system is promising for shuttling therapeutic antibodies to treat central nervous system diseases.**

## 1. Introduction

The clinical success of therapeutic antibodies over the past two decades signals a shift away from conventional drugs toward more targeted antibody-based approaches, particularly in the area of oncology with the development and clinical use of agents such as trastuzumab (Herceptin, Genentech).[1] Trastuzumab (TRA) is a humanized recombinant monoclonal antibody that selectively targets human epidermal growth factor receptor 2 (HER2) in breast cancer cells to induce cell arrest and inhibit cell proliferation. Since its approval in 1998 by the United States Food and Drug Administration, TRA has become the best-in-class agent for controlling local and peripherally metastasized HER2-positive breast cancer.[2] However, adjuvant TRA therapy is associated with an increased incidence of metastasis to the central nervous system (CNS),[3] which is estimated to occur in up to 55% of metastatic HER2-positive breast cancer patients.[4] A major hurdle for antibody-based treatment of brain metastases is the inability of the macromolecules to cross the blood-brain barrier (BBB) and accumulate at therapeutic levels in the metastatic lesions.[5]

The BBB is a physiological barrier at the vascular/CNS interface consisting of a continuous layer of tight junction-expressing endothelia and supporting perivascular cells (i.e., pericytes and astrocytes).[6] It regulates entry of molecules to the brain by restricting passive transport of most molecules across the BBB, with the exception of small (<400 Da) lipid-soluble molecules, while facilitating selective transcellular transport of target molecules via carrier-mediated transport, cation-induced absorptive endocytosis, or receptor-mediate endocytosis.[5c,7] While the BBB structure may be disrupted in the vicinity of brain tumor metastases resulting in increased local BBB permeability, the extent of this disruption is heterogeneous and does not generally permit therapeutic levels of drug entry into the brain.[8] Therefore, development of effective strategies for

Dr. C. He, Dr. J. Li, Dr. P. Cai, T. Ahmed, Prof. J. T. Henderson, Prof. R. Bendayan, Prof. X. Y. Wu
Leslie Dan Faculty of Pharmacy
University of Toronto
144 College Street, Toronto, Ontario M5S 3M2, Canada
E-mail: xywu@phm.utoronto.ca
Dr. W. D. Foltz
STTARR Innovation Centre
Department of Radiation Oncology
Princess Margaret Hospital
Toronto, Ontario M5G 2M9, Canada
Prof. A. M. Rauth
Departments of Medical Biophysics and Radiation Oncology
University of Toronto
Princess Margaret Cancer Centre
610 University Avenue, Toronto, Ontario M5G 2M9, Canada

DOI: 10.1002/adfm.201705668


© 2018 WILEY-VCH Verlag GmbH & Co. KGaA, Weinheim

therapeutic antibody transport across the BBB has been a long-standing challenge in the treatment of CNS disorders including brain metastases of HER2-positive breast cancer.

Various approaches for delivering therapeutic antibodies to the brain have been investigated previously including both invasive and noninvasive methods.[7c,9] Invasive methods such as intracranial injection and convection-enhanced delivery are capable of acute site-specific drug delivery into the brain. However, the use of such systems significantly enhances the requirement of treatment support and the risk of medical complications.[1d,7c,9a] Temporary disruption of the BBB using vasoactive and hyperosmotic agents, or magnetic resonance imaging (MRI)-guided focused ultrasound[10] likewise, has been used to deliver macromolecules into the brain. However, these techniques can be difficult to control spatially and may be problematic for long term (chronic) use.[7c] By contrast, the use of bispecific antibodies and antibody-targeted fusion proteins has demonstrated their utility via noninvasive routes of delivery across the BBB; making them amenable for treatment of chronic disease and repetitive dosing regimens.[5d,9b,11] Typically these constructs incorporate antibody or antibody fragments directed against receptors exhibiting receptor-mediated transcytosis (e.g., insulin receptor (IR), transferrin receptor (TfR)) to gain access to the CNS compartment from the blood. However, clinical use of these agents has been hindered by their rapid liver clearance,[12] low delivery efficiency (i.e., 1:1 molar ratio between targeting and therapeutic antibody), and risk of immunogenicity despite recent advances in generating chimeric, humanized, and fully human antibodies.[13]

Receptor-targeting antibodies (e.g., anti-TfR and anti-IR mAbs) have also been conjugated onto nanoparticles for the delivery of therapeutic agents including peptides and gene constructs to the brain.[14] However, delivery of therapeutic antibodies to brain tumors at therapeutic levels remains challenging. The large molecular size of these antibody constructs makes it difficult to design a nanocarrier system with high payload loading capacity without jeopardizing bioactivity. Conventionally, therapeutic antibodies such as TRA are used to decorate the surface of nanoparticles for targeted drug delivery to specific cancer cells, e.g., HER2 positive cancer cells, instead of utilizing the nanoparticle vector to deliver them. Therefore, a novel nanoparticle system is envisioned that can encapsulate substantial amounts of antibody, shield it from the peripheral circulation, shuttle these agents across the BBB, and release its contents at the tumor site at therapeutic concentrations. Such a nanoparticle system should show advantages over freely diffusible bispecific antibodies and antibody-targeted fusion proteins in terms of facile modification of chemicophysical properties of carrier material, cost effectiveness, loading capacity, immunogenicity, and circulation half-life.[7a,15]

In this work, we present a novel two-step targeted nanoconstruct system made by self-assembly of a polysorbate 80 (PS 80)-containing terpolymer, a lipid, and polymer-bound trastuzumab (TRA–terpolymer nanoparticles (TPN)) for delivering TRA to HER2+ breast cancer cells in the brain. This two-step targeting approach consists of step 1: PS 80-mediated in situ recruitment of apolipoprotein in the circulation to promote receptor-mediated transcytosis across the BBB, followed by step 2: Dissociation of the nanoconstructs in the brain parenchyma to release trastuzumab–polymer chains from the TRA–TPN to enhance local bioavailability of TRA and promote TRA engagement with HER2+ cancer cells (**Figure 1**). The use of PS 80 as a BBB-targeting moiety on nanoparticles is a promising approach due to its low cost, approved use in many injectable pharmaceutical formulations, and demonstrated ability to facilitate nanoparticle transport across the BBB via low-density lipoprotein (LDL) receptor-mediated transcytosis following the adsorption of apolipoproteins in blood plasma[16] enhancing delivery of the therapeutic protein.[17] Additionally, the utilization of the PS 80 moiety may avoid the risk of serious health complications associated with the some antibodies against TfR[11a,18] and human IR.[5c,19] The proposed two-step sequentially targeted nanoconstruct design minimizes TRA exposure in the circulation reducing off-target toxicity,[20] and enhances extracellular TRA engagement with HER2 receptors expressed on the cancer cells after entry into the brain parenchyma. We tested this hypothesis using an in vitro 3D human BBB model and a murine brain metastasis model of HER2+ breast cancer. Results demonstrated the TRA–TPN enabled efficient delivery of bioactive trastuzumab to the brain following intravenous administration, and enhanced anticancer effects against brain metastases in HER2+ breast cancer compared to free trastuzumab.

## 2. Results and Discussion

### 2.1. Formulation and Characterization of Antibody-Loaded Nanoconstructs

A mild self-assembly method was devised to efficiently incorporate immunoglobin G (IgG) antibodies into BBB-penetrating nanoconstructs consisting of a terpolymer and a solid lipid ethyl arachidate stabilized by a surfactant (Figure 1). The terpolymer is comprised of a maltodextrin backbone grafted poly(methacrylic acid) (PMAA) side chains which provide abundant carboxylic acid functional groups for the loading of antibody and fluorescent dye and PS 80 which facilitates nanoparticle transport across the BBB.[9c,16e,f,21] Thus, nanoparticles are designed from biodegradable and generally regarded as safe materials. Fluorescein isothiocyanate (FITC)-labeled immunoglobulin G (IgG–FITC) or the therapeutic antibody TRA was conjugated to the terpolymer via 1-ethyl-3-(3-dimethylaminopropyl)-carbodiimide–N-hydroxysuccinimide (EDC–NHS) covalent coupling (Figure 1a). Successful conjugation was confirmed by the presence of 2.5–3.5 ppm spectral peaks in the $^1$H-NMR (nuclear magnetic resonance) spectra of purified antibody and terpolymer–antibody conjugate, which are absent for the unconjugated terpolymer (**Figure 2**a; Figure S1, Supporting Information). IgG–FITC–TPN and TRA–TPN were synthesized with average particle diameters of ≈100 nm (Figure 2d), polydispersities of ≈0.1–0.2, zeta potential about −47 mV, and an encapsulation efficiency of 100% (Table S1, Supporting Information). Transmission electron micrographs of the nanoparticles revealed their spherical shape and nearly uniform particle size (Figure 2e). The nanoparticles were stable for over 50 h at 37 °C in $\alpha$-MEM (minimum essential medium) supplemented with 50% fetal bovine serum (FBS) (Figure 2f).


© 2018 WILEY-VCH Verlag GmbH & Co. KGaA, Weinheim

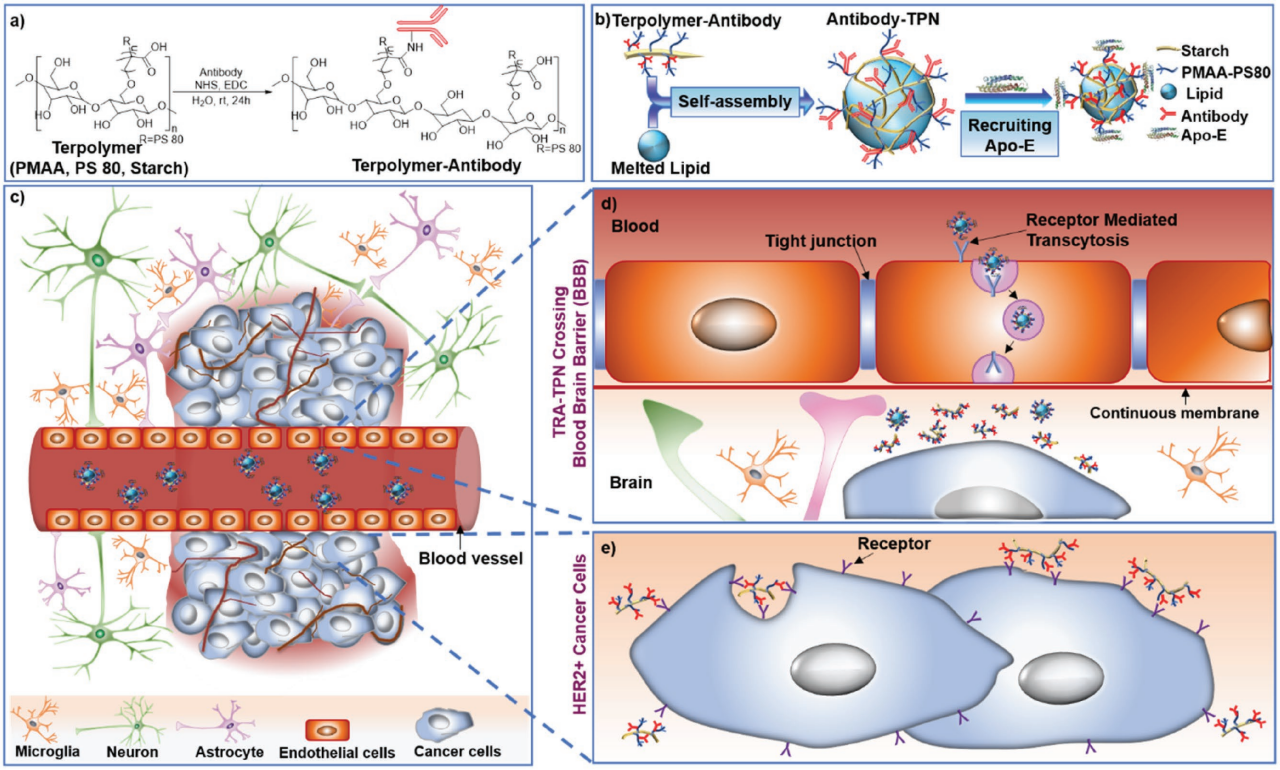


**Figure 1.** a) Structure of PMAA–PS 80-g-St terpolymer and reaction scheme for antibody conjugation. b) Illustration of antibody–TPN self-assembly via microemulsion and probe sonication. c–e) Illustration of the proposed mechanism for delivery of antibody–TPN across the BBB to brain tumor lesions.

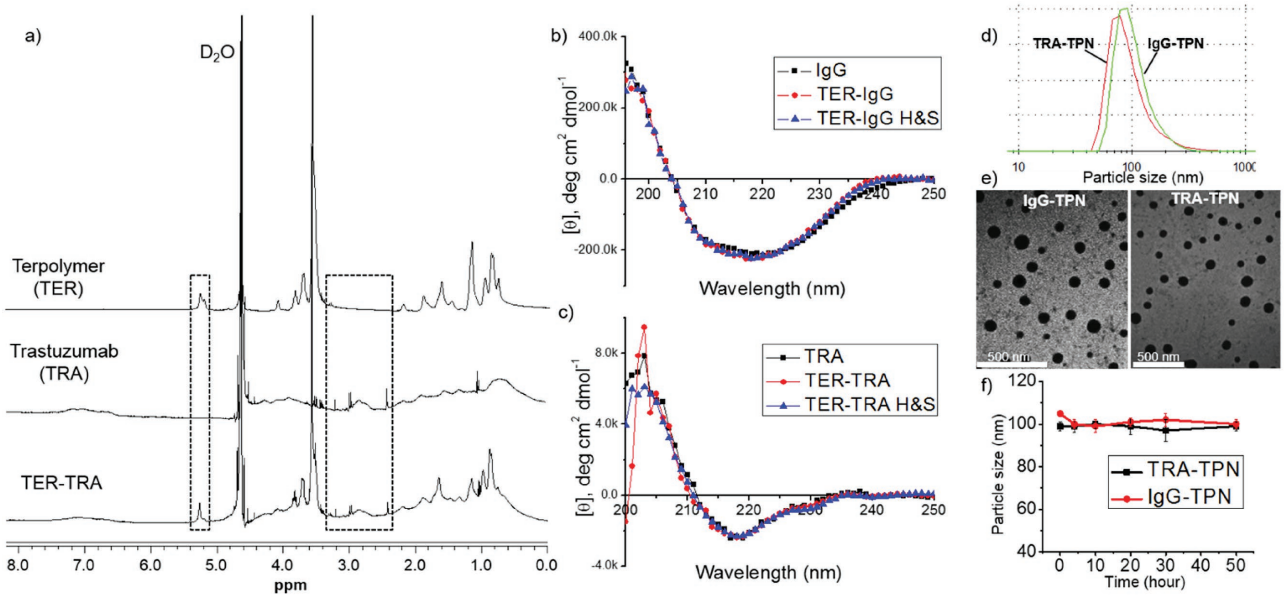


**Figure 2.** Characterization of terpolymer–antibody and antibody–TPN. a) $^{1}$H-NMR characterization. The spectra show the successful conjugation of antibody (trastuzumab: TRA) onto the terpolymer (TER). b,c) Circular dichroism(CD) spectra of antibody (b: IgG, c: TRA), terpolymer–antibody (b: TER–IgG, c: TER–TRA), and terpolymer–antibody after heating and sonication (b: TER–IgG H&S c: TER–TRA H&S). The data show the structure of antibody is stable after conjugation onto terpolymer or microemulsion and probe sonication techniques for the nanoparticles preparation. d) Size distribution (number %) of FITC–IgG–TPN (≈104 nm) and TRA–TPN (≈98 nm). e) TEM images of FITC–IgG–TPN and TRA–TPN. f) Colloidal stability of FITC–IgG–TPN and TRA–TPN over time in $\alpha$-MEM cell medium containing 50% FBS at 37 °C.


© 2018 WILEY-VCH Verlag GmbH & Co. KGaA, Weinheim

### 2.2. Antibody Structure and Function Preserved after Nanoparticle Loading

Structural stability of antibodies is known to correlate with in vivo biological activity including antigen-binding properties. Therefore, antibody secondary structure following conjugation with terpolymer and nanoconstruct synthesis was examined using circular dichroism (CD). Far UV CD spectra of purified IgG–terpolymer conjugate (TER–IgG) and IgG–terpolymer conjugate subjected to elevated temperature (H) and sonication (S) during nanoparticle preparation (TER–IgG H&S: terpolymer–antibody after heating and sonication) were identical to that of native IgG (Figure 2b). The far UV CD spectra of native IgG as well as TER–IgG and TER–IgG H&S are characteristic of IgG's beta-strand structural contributions (Figure 2b).[22] Similarly the characteristics of the far UV CD spectra of native trastuzumab including the minima (zero intensity) at 217 nm and broad shoulder seen at 230 nm remained unchanged following terpolymer (TER–TRA) conjugation, sonication, and elevated temperature exposure (TER–TRA H&S). These results suggest that the secondary structure of IgG and trastuzumab was well preserved during terpolymer conjugation and nanoconstruct preparation (Figure 2c). In addition, in vitro cytotoxicity studies were conducted to further demonstrate that trastuzumab activity was preserved following the preparation process. TRA–TPN and free TRA exhibited comparable dose-dependent cytotoxicity against HER2-positive BT474 human breast cancer cells (Figure S2, Supporting Information: TRA–TPN: 50% inhibitory concentration ($IC_{50} = 0.42 \pm 0.05$ μg mL$^{-1}$; Free TRA: $IC_{50} = 2.1 \pm 0.3$ μg mL$^{-1}$), indicating that the activity of trastuzumab was preserved during the nanoconstruct preparation. Blank nanoparticles (i.e., those without bound antibody) and IgG–TPN did not induce cytotoxicity against BT474 cells at any dose tested. Multivalent binding of antibody-conjugated nanoparticles has been reported to induce coordinated effects in cells, leading an increase in the binding affinity by 10–1000-fold compared to free ligands.[23] Hence, nanoparticle-conjugated therapeutic antibodies could have coordinated effect leading to increased cytotoxicity of TRA–TPN compared to free TRA at the same dose.

### 2.3. In Vitro Uptake of Nanoparticles by Brain Microvessel Endothelial Cells and Transcytosis across an In Vitro BBB Model

Receptor-mediated transport across the BBB first involves binding to receptors on the luminal membrane of brain endothelial cells followed by vesicle-mediated endocytosis/transcytosis to the cell's interior followed by exocytosis from the basolateral membrane to brain parenchyma. To verify the initial two steps of IgG–TPN transport across the BBB, relative levels of IgG–FITC–TPN uptake by rat brain endothelial 4 (RBE4) cells were first determined. IgG–FITC–TPN was taken up by RBE4 cells rapidly in vitro, more than 50% within 30 min, while incubation of free FITC-labeled IgG with RBE4 cells resulted in no detectable uptake over a period of 2 h (**Figure 3**a; Figure S3, Supporting Information).

We subsequently examined BBB uptake in a more sophisticated in vitro 3D human cell model (human brain endothelial cell (HBEC) transwell assay) in order to examine the permeability of both IgG–FITC–TPN and TRA–TPN (Figure 3b,c). This in vitro transwell assay consists of a primary HBEC monolayer cultured on a transwell insert cocultured with a mixed bilayer of human brain pericytes and astrocytes (Figure 3b). Cell monolayers were cultured until a transendothelial electrical resistance (TEER) of 150–300 Ω cm$^2$ was achieved. Treatment with IgG–FITC–TPN or TRA–TPN, introduced to the apical side of the brain microvessel endothelial cells, resulted in permeation of more than 11% of the administered nanoparticles within 30 min, 50-fold greater than that seen for free TRA which permeated less than 0.5% (Figure 3c). These results suggest that these nanoconstructs substantially enhance efficient delivery of both IgG–FITC and TRA across the BBB.

To delineate whether TRA–TPN constructs permeated the BBB as nanoparticles and whether they partially dissociated upon trancytosis (exposing antibody–terpolymer chains to bind HER2+ cancer cells), samples on the top (blood side: plasma) and bottom side (brain side: CNS) of the transwell were collected after a 30 min incubation and imaged via transmission electron microscopy (TEM). Our results indicate that after penetrating the 3D BBB model the morphology of our nanoconstructs was altered (Figure 3d). The smooth dense core nanoparticles collected on the plasma side (blood side) of the matrix were altered to and turned to a less dense, more diffused isoform upon egress to the CNS side (brain side) of the matrix. This apparent partial dissociation of TRA–TPN may result from an erosion of the solid-lipid domain, leading to exposure of the trastuzumab-linked terpolymer chains. This morphological change did not adversely affect trastuzumab cytotoxic activity against HER2+ BT474 cells (Figure 3e). Instead it led to increased TRA binding of the anti-trastuzumab antibody as evidenced by the higher intensity seen in the trastuzumab enzyme-linked immunosorbent assay (ELISA), suggesting increased accessibility of encapsulated trastuzumab following TPN dissociation (Figure 3f,g).

### 2.4. Delivery of Antibody and BBB-Impermeable Dye into Brains of Healthy Mice

The ability of the nanoparticles to extravasate from brain microvessels and enter CNS tissues was initially evaluated in healthy severe combined immunodeficient (SCID) mice in vivo. TPN loaded with FITC-labeled IgG and Hoechst 33342 (a BBB impermeant dye) was administered intravenously to healthy SCID mice and allowed to circulate for 2 h. Treatment with nanoparticles without PS 80 and solutions containing free FITC–IgG and Hoechst 33342 were used as controls. Confocal laser scanning microscopy of brain tissue demonstrated that animals treated with PS 80-containing nanoparticles exhibited abundant staining in neural cell nuclei (**Figure 4**, blue) at sites distant from CNS capillaries (Figure 4, red), and the accumulation of FITC–IgG in CNS tissues outside blood vessels (Figure 4, green). By contrast, treatment with nanoparticles without PS 80, or a mixture of free Hoechst 33342 and IgG–FITC, did not stain cell nuclei in the brain parenchyma, with blue and green FITC–IgG flourescence being constrained to within blood vessel lumen and associated cells (Figure 4). These results demonstrate that PS 80 is essential for nanoparticles extravasation to brain microvessels


© 2018 WILEY-VCH Verlag GmbH & Co. KGaA, Weinheim

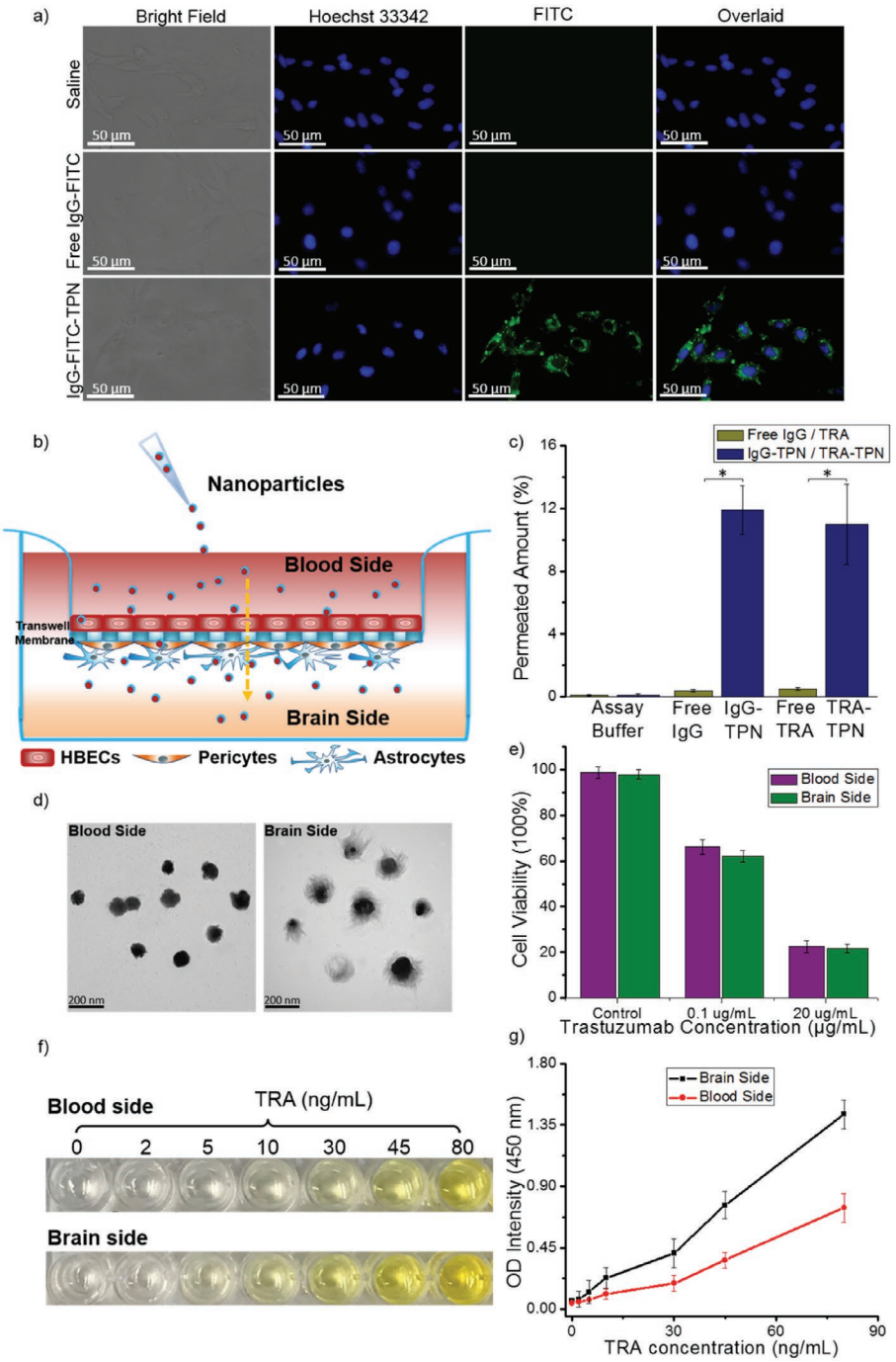


**Figure 3.** a) Uptake of free IgG–FITC, or IgG–FITC–TPN by rat brain endothelial (RBE4) cells and saline control. Fluorescence microscopy images obtained following a 2 h treatment with IgG–FITC–TPN (20 μL, 1 mg $mL^{-1}$ of IgG–FITC) or IgG–FITC. Bright field, cell nuclei stained with Hoechst 33342 (blue), and IgG–FITC conjugate (green) and overlays are shown. b) Schematic of an in vitro human BBB model. Primary human brain endothelial cells were cultured in a transwell insert in contact with cocultured human brain pericytes and astrocytes. The endothelial monolayer was cultured until a TEER value between 150 and 300 Ω $cm^2$ was achieved. c) Permeability of FITC-labeled IgG, FITC–IgG–TPN, TRA, and TRA–TPN across the in vitro human BBB model. Free antibody or antibody–TPN was introduced to the transwell insert (blood side). Following 30 min at 37 °C, permeated free IgG–FITC or IgG–FITC–TPN were quantified using fluorescence spectroscopy, free TRA or TRA–TPN were quantified using commercial trastuzumab quantification ELISA kit. Error bars indicate the standard deviation of three independent experiments. *Statistical significance ($p < 0.05$) as compared to free antibody. d) TEM images of TRA–TPN from blood side or brain side collected from the in vitro BBB model transwell. e) Cytotoxicity of TRA–TPN against BT474 cells after 24 h of incubation. TRA–TPN was collected from blood or brain side of the matrix and incubated with BT474 at two different concentrations (0.1 μg $mL^{-1}$ and 20 μg $mL^{-1}$). Data presented as mean ± SD ($n = 3$). f) TRA–TPN binding ability to anti-trastuzumab antibody. Images of TRA–TPN collected from blood side and brain side (TRA: 2–80 ng $mL^{-1}$) incubated with microplates coated with anti-trastuzumab antibody for 1 h. g) OD intensity ($\lambda = 450$ nm) of TRA–TPN from blood side and brain side (TRA: 2–80 ng $mL^{-1}$) incubated with microplates coated with anti-trastuzumab antibody for 1 h. Data presented as mean ± SD ($n = 3$).


© 2018 WILEY-VCH Verlag GmbH & Co. KGaA, Weinheim

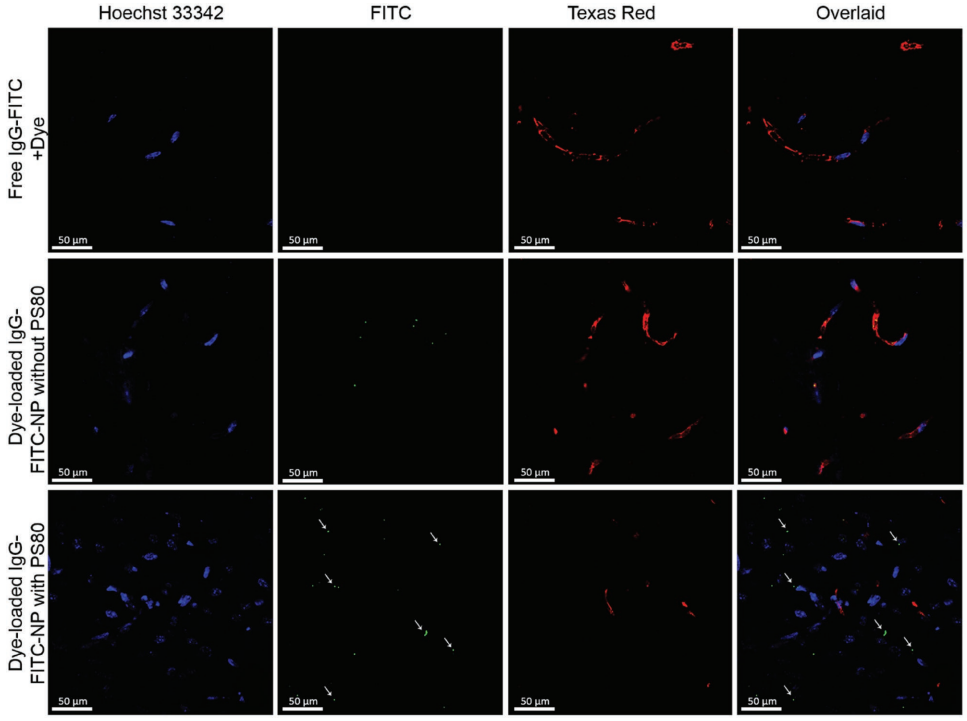


**Figure 4.** Representative laser scanning confocal microscopic images of healthy SCID mouse brain sections following i.v. administration of free IgG–FITC and Hoechst 33342, Hoechst 33342 loaded within IgG–FITC–NP (without PS 80), or Hoechst 33342 loaded within IgG–FITC–TPN (with PS 80). All treatments were administered with an equivalent dose of 0.5 mg Hoechst33342 and 0.2 mg IgG–FITC. Mice were treated for 2 h. Texas red-dextran was administered to the mice i.v. 15 min before euthanasia. Hoechst 33342-labeled cell nuclei appear blue. Texas red-dextran appears as red. IgG–FITC appears as green. Arrows: indicating representative nuclei and FITC–IgG–TPN located away from blood vessels. Scale bar = 50 µm for all images.

in order to deliver BBB-impermeable antibodies or dye agents to brain parenchyma. This finding is consistent with previous reports that PS 80 enables ApoE coating and thereby transcytosis of nanoparticles through the BBB via low density lipoprotein receptor-related protein 1-mediated endocytosis.[16c]

### 2.5. Biodistribution and Brain Accumulation of TRA–TPN in Mice with Brain Metastases of HER2-Positive Breast Cancer

Our brain metasis model was established through the sterostatic intracranial injection of HER2+ BT474 human breast cancer cells into immune-deficient SCID mice. Resulting brain tumor metastases were allowed to grow and overall tumor growth monitored using in vivo MRI. One month following stereotactic implantation, TRA–TPN conjugates containing HiLyte Fluor 750 hydrazide (HF750) and fluoresceinamine isomer I (FA) fluorescence dyes were injected intravenously into tumor-bearing mice and nanoparticle accumulation at tumor sites was monitored using whole-body near-infrared fluorescence imaging for up to 2 h (**Figure 5**a). Nanoparticles were detectable in the brain as early as 15 min postinjection and remained for at least 2 h, which was also confirmed by ex vivo fluorescence imaging of resected brains 2 h following treatment (Figure 5b). Ex vivo fluorescence imaging also showed substantial signal of HF750-labeled terpolymer in the kidneys, suggesting that the dissolved polymer chains were largely eliminated via this route (Figure 5c). Laser scanning confocal microscopy of the tumor-bearing brain tissue sections revealed that the FA-labeled TRA–TPN (green) were able to extravasate from the blood vessel lumen (red) and accumulate within tumor lesions in the brain, while free FA-labeled TRA did not (Figure 5d).

### 2.6. Quantification of Trastuzumab Accumulation in Healthy Brain and Tumor-Bearing Brain

To quantify TRA accumulation in the brains of treated animals, 2 h following i.v. injection of 40 mg $kg^{-1}$ free trastuzumab or an equivalent dose of TRA–TPN, whole brains of healthy or tumor-bearing mice were perfused with saline, resected, and homogenized for assay using a commercial TRA ELISA kit. As expected, free TRA reached the brain at negligible levels 2 h following injection owing to its large molecular weight (≈150 kDa) and polar nature, though its concentration in the brain of tumor bearing brains was 4-fold that seen in the healthy brains likely due to the impaired vascular network surrounding CNS tumors. By contrast, treatment with TRA–TPN resulted in 40-fold and 50-fold increased TRA levels in the healthy brains and tumor-bearing brains, respectively (Figure 5e,f). These data confirmed the pivotal role of this first step targeting of LDL-R and receptor-mediated transcytosis play in relaying the TPN shuttle payload.

Previously Lockman et al. have demonstrated that while the BBB in >89% of brain metastasis of breast cancers were more permeable to chemotherapeutic drugs, drug accumulation at cytotoxic concentrations was only achieved in roughly 10% of


© 2018 WILEY-VCH Verlag GmbH & Co. KGaA, Weinheim

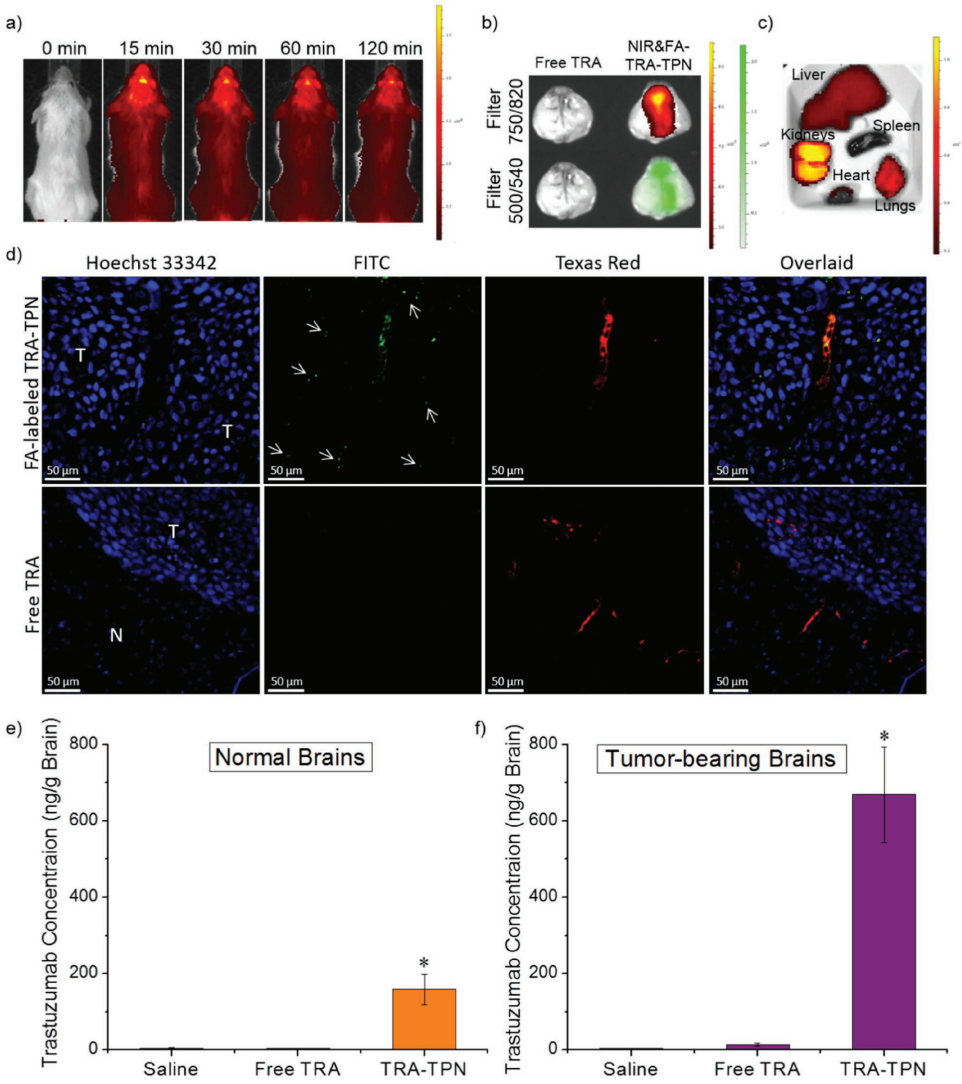


**Figure 5.** Biodistribution of fluorescence-labeled nanoparticles in SCID mice with brain metastases of human HER2 positive breast cancer cells. a) Representative near-infrared fluorescence whole body images showing brain tumor accumulation of TRA–TPN after i.v. injection. b) Representative ex vivo fluorescence image of the dissected whole brain and c) organs 2 h after injection of TRA–TPN labeled with both HF 750 and FA (HF 750 filter ($\lambda_{ex/em}$ = 750/820 nm); FITC filter ($\lambda_{ex/em}$ = 500/540 nm). d) Confocal microscopic images of brain tissue sections 2 h after i.v. injection of FA-labeled TRA–TPN (top panels) or free FA-labeled TRA (bottom panels). FA-labeled TRA shown in green. Texas red-dextran, shown in red, was administered to the mice i.v. 15 min before euthanasia. Hoechst 33342-stained cell nuclei shown in blue (T: brain tumor area; N: normal area without tumor). Arrows point to representative FA-labeled TRA–TPN away from blood vessels and accumulated into microscopic tumor lesions. Scale bar = 50 µm for all image. e,f) ELISA quantification of trastuzumab (TRA) in brains (see the Experimental Section for details). The concentration of TRA in healthy SCID mouse brains and HER2 positive tumor-bearing SCID brains at 2 h after i.v. injection is shown. Mice were treated by a single intravenous administration of saline, free TRA, or TRA–TPN (40 mg kg$^{-1}$, $n$ = 3). *Statistical significance ($p < 0.05$) as compared to free TRA treated groups. Error bars indicate the standard deviation of three independent experiments.

these lesions.[8] Therefore, it is thought that even if compromised, the BBB remains a significant barrier to drug delivery to brain metastases especially for macromolecules.

### 2.7. Treatment with TRA–TPN Enhanced Apoptosis of HER2+ Cancer Cells in Mouse Brain Tumor Lesions

To examine whether the TRA–TPN shuttled TRA caused cancer cell apoptosis (an early indicator of therapeutic drug efficacy), brain sections were taken from tumor-bearing SCID mice 24 h following i.v. injection of free TRA or TRA–TPN (40 mg kg$^{-1}$) and stained for both activated caspase-3 (**Figure 6**a) and terminal deoxynucleotidyl transferase deoxyuridine triphosphate (dUTP) nick end labeling (TUNEL) (Figure 6b). Consistent with the data seen for trastuzumab accumulation in the brains, free TRA did not elicit a higher number of apoptotic tumor cells compared to saline controls (Figure 6a,c). By contrast, treatment with TRA–TPN led to a greater than 4-fold increase in caspase-3 positive tumor cells per mm$^2$ compared to saline and free trastuzumab groups (Figure 6a,c). Similarly a 4-fold increase in the number of TUNEL-(+) cells


© 2018 WILEY-VCH Verlag GmbH & Co. KGaA, Weinheim

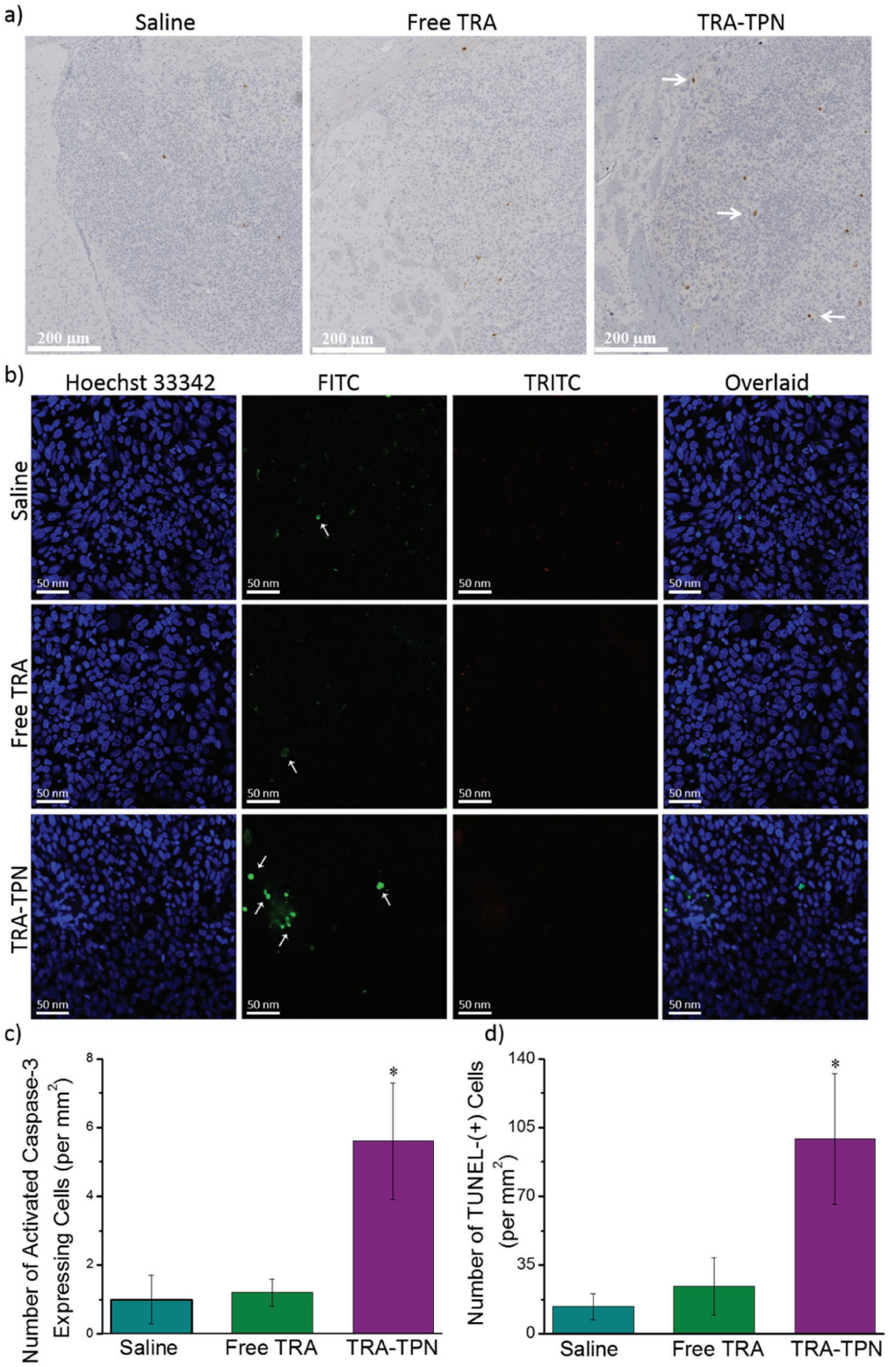


**Figure 6.** a) Brain sections prepared from BT474 brain metastasis model tumor-bearing SCID mice 24 h post i.v. injection of free TRA or TRA–TPN and stained for activated caspase-3. b) TUNEL assay for apoptosis in BT47E cells of brain metastasis tumor model. Tumor-bearing brain sections prepared from mice 24 h following intravenous injection of saline ($n = 3$), free TRA (40 mg kg$^{-1}$, $n = 3$), or TRA–TPN (40 mg kg$^{-1}$, $n = 3$) (caspase 3+ cells shown in brown and FITC-labeled TUNEL-(+) cells shown green (arrows)). c) Quantification number of activated caspase-3 expressing cells per mm$^2$ and d) TUNEL-(+) cells per mm$^2$. (*)Statistically significant (*$p < 0.05$) as compared to free TRA treated groups. Error bars indicate the standard deviation of three independent experiments.


© 2018 WILEY-VCH Verlag GmbH & Co. KGaA, Weinheim

was observed throughout large metastatic brain tumors following treatment with TRA–TPN compared to free trastuzumab (Figure 6b,d). These results suggest that i.v. injected TRA–TPN are able to not only deliver substantial amounts of TRA to brain tumor metastasis, but occur at sufficient levels to induce local bioactivity against HER2+ breast cancer cells.

### 2.8. Treatment with TRA–TPN Inhibits Growth of HER2+ Brain Tumors and Extends Survival of Tumor-Bearing Mice

To evaluate therapeutic efficacy of TRA–TPN, SCID mice with brain metastases of HER2-positive human breast cancer were treated with equivalent doses of TRA–TPN ($4 \times 10$ mg kg$^{-1}$ TRA, i.v.), free TRA ($4 \times 10$ mg kg$^{-1}$ TRA, i.v.) or saline once per week over a 4-week period (**Figure 7**a). Tumor treatment was typically initiated one month after stereotactic tumor injection into the brain. The general health and body weight of mice were monitored over the course of the 80-day experiment time. The brain tumor size as measured using in vivo MRI was monitored for up to 42 d. Brain tumor-bearing mice treated with saline or free TRA exhibited the most rapid tumor growth (Figure 7b,c) and had similar mean survival times of 39 and 42 d, respectively (Figure 7d). By contrast, treatment with TRA–TPN inhibited tumor growth by 43-fold with a tumor growth

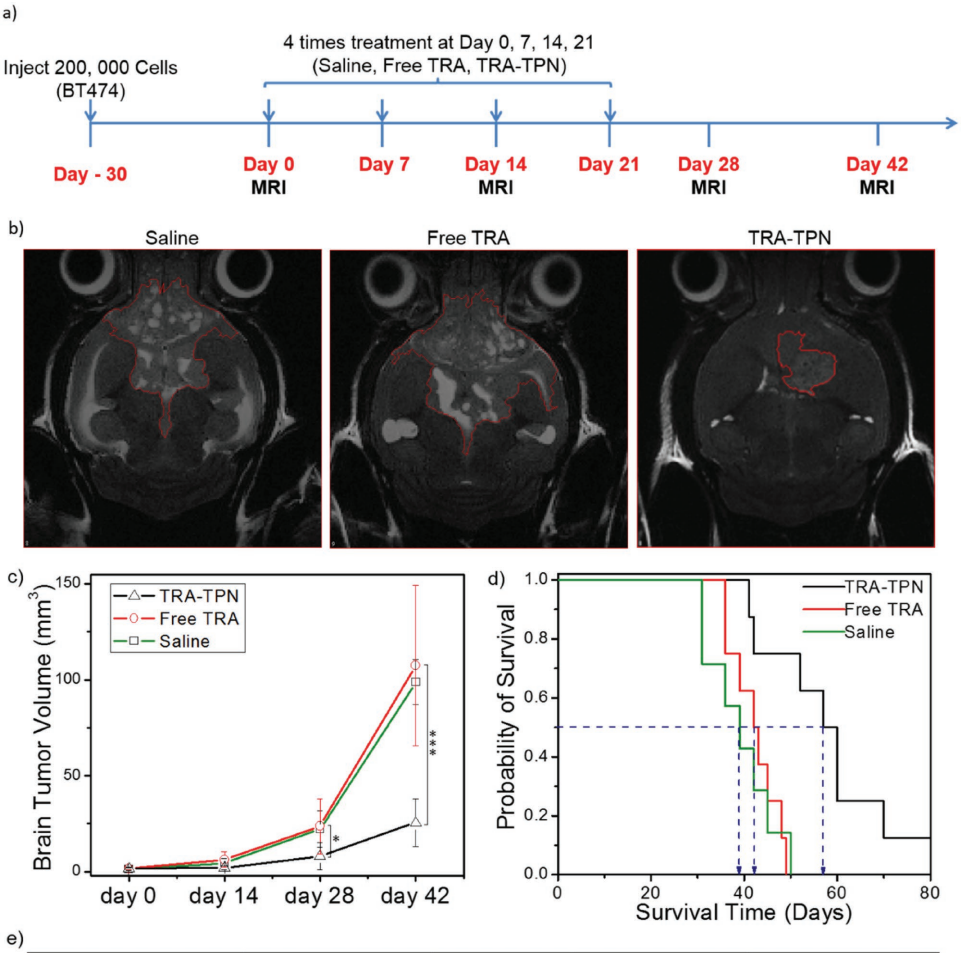


e)

| Groups | Tumor Growth Inhibition (TGI % on day 42) | Mean Survival (Days) | Median Survival Time (MST) (Days) | Percentage Increase in Life Span (ILS %) (Days) |
|---|---|---|---|---|
| Saline (n=7) | n/a | 39±7 | 39 | / |
| Free TRA (n=8) | 1.6 ± 1 | 42±5 | 42 | 7.7 |
| TRA-TPN (n=8) | 70.2 ± 5 | 57±12 * | 57 | 46.2 |

**Figure 7.** Inhibition of brain tumor growth and animal survival. a) Schedule of treatment and imaging of brain tumor-bearing mice with IV injected free TRA or TRA–TPN (10 mg kg$^{-1}$ TRA, $n = 8$) with saline as control ($n = 7$). b) In vivo MRI images of brain tumor 42 d after the start of treatment ($4 \times 10$ mg kg$^{-1}$ TRA, $4 \times 10$ mg kg$^{-1}$ TRA–TPN, or $4 \times 200$ µL saline over a 4-week period). Red lines outline extent of tumor spread. c) Normalized increase in the total tumor volume. (*: $p < 0.05$; ***: $p < 0.001$) Statistically significant as compared to free TRA treated groups (all treated mice were survived on day 28; on day 42, the numbers of survived mice for free TRA and TRA–TPN treated groups were 5, 6, respectively). d) Kaplan–Meier survival curve of tumor-bearing mice following treatment (Saline: $n = 7$, free TRA: $n = 8$; TRA–TPN: $n = 8$). e) Effect of treatment on tumor growth inhibition (TGI% on day 42), mean survival days, median survival time (MST), and percentage increase in life span (ILS%) of brain tumor bearing mice. All data presented as mean ± SD. (*) Statistically significant ($p < 0.05$) as compared to free TRA treated groups.


© 2018 WILEY-VCH Verlag GmbH & Co. KGaA, Weinheim

inhibition (TGI) of 70.2% as compared to free TRA with a TGI of 1.6%, prolonged the median survival time of tumor-bearing mice by more than 1.3-fold, and increased the percentage of life span by 6-fold compared to treatment with an equivalent dose of free trastuzumab (Figure 7d). As demonstrated above, the improved therapeutic effect of TRA–TPN may be due to its two-step targeting capabilities. The active binding of TRA–TPN with LDL-R enables receptor-mediated transcytosis allowing passive accumulation of TRA–TPN at tumor sites through the EPR effect. Following brain entry, the TRA–TPN undergoes gradual dissociation (Figure 3), exposing and releasing trastuzumab–polymer conjugate which selectively targets HER2 on the cancer cells, thus generating a higher therapeutic impact.

### 2.9. Treatment with TRA–TPN in Tumor-Bearing Mice Did Not Induce Histological Changes of the Major Organs

To evaluate the possible acute toxicity of TRA–TPN treatment on major organs, histological sections were cut through these tissues and stained with hematoxylin-eosin from lungs, liver, kidneys, and heart of tumor-bearing mice treated with $4 \times 10$ mg kg$^{-1}$ TRA–TPN or an equivalent dose of free TRA at the end points of the experiment. These tissue sections showed no histological abnormalities in any of the major organs as compared to saline controls (Figure S4, Supporting Information). Thus TRA–TPN improved therapeutic efficacy compared to free TRA treatment groups without inducing histological changes in the major organs at the administered dosing level and regimen.

## 3. Conclusion

A novel two-step targeted nanoconstruct system for shuttling therapeutic antibody trastuzumab to HER2+ breast cancer cells grown in the mouse brain is reported. The system first exploits the BBB-penetrating PS 80-containing terpolymer to enter the brain parenchyma by receptor-mediated trancytosis; and then uses the gradual dissociation of the particle to expose encapsulated TRA for targeting HER2+ cancer cells to exert its therapeutic effect. Efficient loading of antibody was achieved while preserving the structure and function of the antibody. BBB-penetration of the nanoconstructs was demonstrated in vitro using a 3D human BBB model and in the brains of healthy mice and a mouse model of brain metastases of human HER2+ breast cancer following intravenous administration. TRA–TPN were shown to accumulate within brain tumor lesions and delivered 40- to 50-fold greater amounts of trastuzumab to the brain compared to free trastuzumab. Treatment of brain tumor-bearing mice with 40 mg kg$^{-1}$ TRA–TPN enhanced tumor cell apoptosis by 4-fold after 24 h, significantly inhibited tumor growth by 43-fold and prolonged median survival time by more than 1.3-fold compared to an equivalent dose of free trastuzumab, without inducing histological changes in the major organs. These results suggest that the two-step targeted nanoconstruct system is a promising approach for the noninvasive delivery of biological macromolecules, including therapeutic antibodies, for the treatment of diseases in the brain.

## 4. Experimental Section

*Materials*: Soluble starch, maltodextrin (dextrose equivalent = 16.5–19.5), methacrylic acid, sodium thiosulfate, potassium persulfate, PS 80, sodium dodecyl sulphate, dimethyl sulfoxide, Pluronic F-68 (PF68), FA, *N*-(3-dimethylaminopropyl)-*N*′-ethylcarbodiimide hydrochloride (EDC), NHS, ethyl arachidate, IgG–FITC conjugate, and all other chemicals unless otherwise mentioned were purchased from Sigma-Aldrich Canada (Oakville, ON, Canada). HiLyte Fluor 750 hydrazide (HF 750) was purchased from AnaSpec (Fremont, CA, USA). Hoechst 33342 and Texas red-labeled dextran (MW 70 000 Da) were obtained from Life Technologies (Carlsbad, CA, USA). Trastuzumab was purchased from BOC Sciences (Shirley, NY, USA). Trastuzumab ELISA kit was purchased from MyBiosource (San Diego, CA, USA). RBE4 cells were provided by Dr. Bendayan. BT474 cells were obtained from American Type Culture Collection (Manassas, VA, USA) and were confirmed to be pathogen free by the supplier using IMPACT Profile I polymerase chain reaction. These cells were passaged for less than six months following recovery from frozen samples. The 3D human blood brain barrier model was purchased from Alphabioregen (Boston, MA, USA).

*Synthesis and Characterization of Antibody-Linked PMAA–PS 80-g-St Terpolymer*: A terpolymer of poly(methacrylic acid) and polysorbate 80 grafted starch (PMAA–PS 80-g-St) was prepared using a method described previously.[24] Antibody (i.e., FITC-labeled IgG or TRA) was covalently linked to the purified PMAA–PS 80-g-St by EDC/NHS coupling (Figure 1a).[16e,f] Briefly, 500 mg of purified PMAA–PS 80-g-St, 50 mg of EDC, and 50 mg of NHS were dissolved in 3 mL of distilled deionized water (DDIW) and allowed to react for 2 h at room temperature. Antibody solution (100 µL, 20 mg mL$^{-1}$, phosphate buffered saline (PBS), pH 7.4) was added to the activated terpolymer solution and allowed to react at 37 °C for 24 h. The product solution was neutralized to pH 7.4 using 0.1 N NaOH, and purified by extensive resuspending and filtered by Nanosep 300K Omega centrifuge filters (Sigma-Aldrich, Canada). The purified product was then lyophilized and stored in a desiccator at 4 °C.

Successful conjugation of antibody to the terpolymer was characterized using 400 MHz $^1$H NMR spectrometer (Varian Mercury 400, Department of Chemistry, University of Toronto). Terpolymer, antibody, and terpolymer–antibody conjugate samples were dispersed in deuterated water in standard NMR tubes and spectra were acquired according to standard proton pulse sequences. The IgG–FITC content conjugated onto terpolymer was determined to be 35 µg per 1 mg of terpolymer using ultraviolet–visible (UV–Vis) spectrometer (Agilent 8453, 490 nm). The TRA content conjugated onto terpolymer was measured using a commercial TRA ELISA kit, and was determined to be 33 µg per 1 mg of terpolymer.

*Preparation and Characterization of Antibody-Loaded Terpolymer Nanoparticles*: In a typical experiment, 15 mg of ethyl arachidate was added to a 15 mL conical tube and heated to 45 °C. 50 µL of 100 g L$^{-1}$ PF68 solution, and 300 µL of 100 mg mL$^{-1}$ purified antibody–terpolymer conjugate solution were added to the solution and stirred for 20 min. The mixture was sonicated for 10 min using a Hielscher UP 100H probe ultrasonicator (Ringwood, NJ, USA) at 80% peak power. Following sonication, the entire emulsion was immediately transferred into 1 mL of cold saline (0.9% w/v NaCl) and stirred on ice. The particle size and zeta potential of the TPN was characterized using a Malvern Zetasizer Nano ZS (Worcestershire, UK). Immediately following formulation, the nanoparticle suspension (NP) was diluted 4 times by PBS (pH = 7.45), transferred to a centrifugal filter unit with a pore size of 0.1 µm, and centrifuged for 5 min at a 10 000 min$^{-1}$ (rpm). The free antibody–terpolymer concentration in the filtrate was assayed at 490 nm (FITC–IgG) or 235 nm (TRA) using a UV–Vis spectrometer (Agilent 8453) to determine the drug encapsulation efficiency (%wt drug/wt total drug). For TEM, TPN solution in DDIW was dried onto a carbon coated grid. The TEM images were acquired using a Hitachi H7000 electron microscope (Hitachi Canada, Ltd., Mississauga, Ontario, Canada) with an accelerating voltage of 100 kV. To determine the stability of the antibody-loaded TPN (Antibody-TPN), 200 µL of NP were incubated in 2 mL of $\alpha$-MEM cell medium containing 50% FBS for up to 50 h at 37 °C.


© 2018 WILEY-VCH Verlag GmbH & Co. KGaA, Weinheim

Aliquots were taken at various time intervals and diluted with DDIW for analysis of particle size and zeta potential (Malvern Zetasizer Nano ZS).

*Characterization of Antibody Structure*: Far UV CD spectroscopy (200–260 nm) was used to assess the secondary structure of native antibody (i.e., IgG and trastuzumab) and antibody–terpolymer conjugate following heating and sonication conditions used in nanoparticle preparation. The CD spectra were measured using a circular dichroism spectropolarimeter (Jasco J-810, MD, USA) equipped with a Peltier temperature controller operated at 25 °C. Samples were scanned at 1 nm intervals between 200 and 260 nm using an 8 s response time. Measurements were repeated three times and averaged.

*Uptake Kinetics of Terpolymer Nanoparticle in Rat Brain Endothelial Cells and Permeability of Terpolymer Nanoparticle in a Human Blood Brain Barrier Model*: RBE4 cells were seeded at a density of 10 000 cells per well in 24-well plates and incubated for 24 h at 37 °C under 5% $CO_2$. The medium in each well was replaced with 1 mL of fresh culture medium containing 20 µL of FITC–IgG–TPN or an equivalent dose of FITC-labeled IgG, and incubated at 37 °C for up to 2 h. At various incubation times, the nanoparticle-containing medium was removed from the wells and the cells were washed three times with cell culture medium. Cell nuclei were stained with 0.5 µg mL$^{-1}$ of Hoechst 33342 (Molecular Probes, Inc. Eugene, OR, USA). The cells were imaged on an AMG EVOSf1 fluorescence microscope (Invitrogen, Carlsbad, CA, USA) with the filters for FITC (Ex./Em. = 490/520 nm) and for Hoechst 33342 (Ex./Em. = 360/447 nm). The fluorescent intensity was measured using a microplate fluorescence reader ($\lambda_{ex}$ = 500 nm, $\lambda_{em}$ = 530 nm) to quantify the cellular uptake of the IgG–FITC–TPN.

An in vitro 3D human BBB transwell coculture assay (Alphabioregen, Boston, MA, USA) was used to assess the BBB permeability of antibody–terpolymer nanoparticles. The assay consists of a primary human brain endothelial cell monolayer, cultured on a transwell insert, cocultured with human brain pericytes and human astrocytes. Permeability experiments were performed following the manufacturer's protocol. The endothelial cell monolayer was kept in culture until a TEER value between 150 and 300 Ω cm$^2$ was achieved. Culture medium in the insert (apical side) was replaced with 200 µL of assay buffer containing 1 mg mL$^{-1}$ of FITC-labeled IgG (or free TRA) or an equivalent dose of IgG–FITC–TPN (or TRA–TPN) buffer, while culture medium in the assay plate wells was replaced with 900 µL of fresh medium (basolateral side). The plate was placed on a shaker (100 rpm) and incubated at 37 °C at 5% $CO_2$ for 30 min. The fluorescent intensity of FITC-labeled IgG was measured using a microplate fluorescence reader ($\lambda_{ex}$ = 500 nm, $\lambda_{em}$ = 530 nm) after incubation and the concentration of FITC–IgG or FITC–IgG–TPN was determined with respect to the appropriate calibration curve. The amounts of TRA in the top chamber of the transwell (blood side) or the bottom chamber (brain side) were quantified using the TRA Quantification ELISA kit as per the manufacturer's protocol (MyBiosource).

*Examination of Morphological Change of Nanoconstructs after BBB Permeation Test by TEM*: TPN solution collected from blood side and brain side was further tested by TEM. The nanoparticles solution was dried onto a carbon coated grid. The TEM images were acquired using a Hitachi H7000 electron microscope with an accelerating voltage of 100 kV.

*Animal Model*: All animal handling and procedures were conducted under an approved protocol from the Animal Care Committee at the Ontario Cancer Institute. An animal model for brain metastasis of breast cancer was established by injecting human breast cancer cells (BT474) ($20 \times 10^4$ cells per mouse) intracranially into the cortex of four to six weeks old, SCID mice (Ontario Cancer Institute, Toronto, ON, Canada) using a stereotaxic system (SAS-5100, ASI Instruments, Warren, MI, USA).

*Delivery of BBB-Impermeable Dye into Healthy Mouse Brain*: Hoechst 33342-loaded IgG–FITC–terpolymer nanoparticles (IgG–FITC–TPN) were prepared using the same method as described above. A mixture of 250 µL of Hoechst 33342 solution (10 mg mL$^{-1}$), 300 µL of IgG–FITC–terpolymer solution (100 mg mL$^{-1}$), 50 µL of PF 68 solution (100 mg mL$^{-1}$), and 15 mg of ethyl arachidate was heated to 45 °C and stirred for 20 min. TPN was formed under ultrasonication using a Hielscher UP100H probe ultrasonicator for 10 min and suspended in sterile 5% dextrose to a final Hoechst 33342 concentration of 2.5 mg mL$^{-1}$.

To examine nanoparticle penetration into healthy brain, SCID mice were treated with 200 µL of Hoechst 33342-loaded IgG–FITC–TPN with PS80 (2.5 mg mL$^{-1}$ dye), 200 µL of Hoechst 33342-loaded IgG–FITC–NP without PS80 (2.5 mg mL$^{-1}$ dye), or the mixture of free IgG–FITC and Hoechst 33342 (IgG–FITC: 1.0 mg mL$^{-1}$; Hoechst 33342: 2.5 mg mL$^{-1}$ in saline) via tail vein injection. Mice were euthanized 2 h following treatment. Texas red-labeled dextran (100 µL volume, 1 wt% solution) was administered intravenously 15 min prior to euthanasia. The brain was dissected, fixed in 10% formalin for 3 h, transferred to 30% dextrose solution overnight, embedded in Tissue-Tek OCT resin (Somagen, Torrance, CA, USA), and finally flash frozen. Thaw mounted 20 µm thick frozen sections were prepared using a Leica CM3050S cryostat (Leica, Wetzlar, Germany) and analyzed using a Zeiss LSM700 confocal microscope (Carl Zeiss, Jena, Germany) using fluorescent excitation and emission filters appropriate for detection of the indicated chromophores (Dextran, Texas Red: Ex./Em. = 595/615 nm; FITC: Ex./Em. = 490/520 nm; Hoechst 33342: Ex./Em. = 352/461 nm).

*Trastuzumab Quantification in Healthy Brains and Tumor-Bearing Brains*: TRA–TPN (40 mg kg$^{-1}$ TRA) or free TRA (40 mg kg$^{-1}$ TRA) were administered via lateral tail vein injection into healthy SCID mice with the BT474 brain metastases model of breast cancer (typically four weeks following tumor inoculation). The mice were euthanized 2 h following treatment. Following perfusion with ice-cold saline via the left ventricle, their brains were harvested and homogenized in 10 mL of radioimmunoprecipitation (RIPA) buffer (1× RIPA buffer, pH 8.0, Sigma-Aldrich) per 1 g of brain tissue. The homogenate was supplemented with 100 µL of 1× protease inhibitor mixture, and 200 µL each of 1× phosphatase inhibitor mixtures 1 and 2 (Sigma-Aldrich) per 10 mL of ice-cold buffer. Homogenized tissue samples were placed on a platform rocker for 1 h at 4 °C, and then supernatant fractions were prepared by centrifugation at 14 100 × g for 30 min at 4 °C. The amount of TRA in the samples was quantified using the TRA Quantification ELISA kit as per the manufacturer's protocol (MyBiosource).

*Apoptosis in Tumor-Bearing Brain Tissue*: To investigate brain tumor cell apoptosis following treatment with TRA-loaded nanoparticles or free TRA, 200 µL of TRA–TPN (40 mg kg$^{-1}$ trastuzumab) or an equivalent dose of free TRA was administered via lateral tail vein injection into SCID mice with the BT474 brain metastases model of breast cancer (typically four weeks following tumor inoculation). The mice were euthanized 24 h following treatment. The brain samples were bisected along their midline and postfixed in 4% paraformaldehyde IN, 0.1 M PBS overnight at 4 °C. Specimens were then removed from fixation, flushed, and equilibrated in 30% sucrose at 4 °C, embedded in Tissue-Tek OCT resin (Somage) and finally flash frozen. Thaw mounted 10 µm thick frozen sections were obtained on a Leica, model CM3050S cryostat. Tumor cell apoptosis was determined by the TUNEL reaction (TdT In Situ Apoptosis Detection Kit, R&D Systems, Minneapolis, MN, USA) and immunofluorescent labeling of cleaved caspase-3. The TUNEL reaction product was visualized with streptavidin–biotin–FITC complex at 10× magnification. Apoptotic TUNEL-(+) and Caspase 3+ cells were imaged using a Nikon Eclipse E1000 motorized microscope equipped with a 270° rotating stage, Nomarski contrast optics, and fluorescent excitation and emission filters appropriate for detection of the indicated chromophores (DAPI (4′,6-diamidino-2-phenylindole): Ex./Em. 358/461 nm, FITC: Ex./Em. 470/525 nm) (Nikon, Tokyo, Japan). Images were captured using a Hamamatsu C4742-95 camera (Hamamatsu, SZK, Japan). Measurement of TUNEL-(+) and caspase-3-(+) cells was performed on >2 visual fields per brain. The number of apoptotic cells within each field was normalized to the tumor area, and this was averaged for each animal for statistical analysis. The number of apoptotic cells for each treatment was taken as the average of the animal normalized apoptotic cell numbers.

*Evaluation of Therapeutic Efficacy*: SCID mice with implanted brain metastases of HER2+ BT474 breast cancer received intravenous injections of saline, free TRA, TRA–TPN (10 mg of TRA per kg body


© 2018 WILEY-VCH Verlag GmbH & Co. KGaA, Weinheim

weight, 200 µL injection volume) on day 0, typically one month after tumor inoculation. Three more identical treatments were administered on day 7, 14, and day 21. Tumor growth was monitored in vivo using MRI, once every two weeks following the first treatment. MRI was performed at the STTARR Facility (University Health Network, Toronto, Canada) using a 7 Tesla Biospec (Bruker Corporation, Ettlingen, DE) equipped with dedicated mouse brain imaging hardware, providing a stack of 2D coronal T2-weighted images at 100 × 100 × 500 µm spatial resolution. The tumor volume (TV) was quantified from the MRI images using MIPAV (Medical Image Processing, Analysis, and Visualization, NIH) software based on the manual segmentation of the volume of interest across the stack of 2D images. Tumor growth inhibition (TGI) was calculated from the tumor volume of each group according to

$$\mathrm{TGI}\,(\%) = \frac{\mathrm{TV\ control} - \mathrm{TV\ treated}}{\mathrm{TV\ control}} \times 100\% \quad (1)$$

Animal survival time was evaluated by the mean survival time and median survival time (MST), and the percentage increase in life span (ILS%) was calculated as

$$\mathrm{ILS}\,(\%) = \left(\frac{\mathrm{MST\ treated}}{\mathrm{MST\ control}} - 1\right) \times 100\% \quad (2)$$

Mice were euthanized by cervical dislocation under 1% isofluorane anesthesia at the clinical endpoint, defined by signs of discomfort (i.e., 20% weight loss, lack of grooming, signs of self-mutilation, resistance to ambulation). Immediately after euthanasia, intact hearts, livers, lungs, and kidneys were fixed in 10% neutral-buffered formalin, paraffin-embedded and stained with haematoxylin and eosin for morphological evaluation, which was conducted by a a board-certified veterinary anatomic pathologist.

*Statistical Data Analysis*: Statistical software (OriginPro8) was used for statistical analysis. All data are presented as means ± standard deviation (SD) from three independent trials unless otherwise indicated. Student's *t*-test was utilized to determine statistical significance between two groups. $p$ values < 0.05 were considered statistically significant.

## Supporting Information

Supporting Information is available from the Wiley Online Library or from the author.

## Acknowledgements

C.H., J.L., and P.C. contributed equally to this work. The authors gratefully thank the University of Toronto Connaught Innovation Award and the Natural Sciences and Engineering Research Council (NSERC) of Canada for the Discovery and the Equipment Grants to X.Y.W.; the scholarships from NSERC of Canada, Ontario Graduate Scholarship, and the Department of Pharmaceutical Sciences at the University of Toronto to J.L; the Connaught International Scholarship for Doctoral Students at the University of Toronto to T.A. The authors also thank Dr. Md. T. Hoque (Department of Pharmaceutical Sciences, Leslie Dan Faculty of Pharmacy, University of Toronto) for assisting the measurement of TEER value, and the Spatio-Temporal Targeting and Amplification of Radiation Response (STTARR) program and its affiliated funding agencies for providing the imaging facilities.

## Conflict of Interest

The authors declare no conflict of interest.

## Keywords

blood-brain barrier, brain metastasis, breast cancer, hybrid nanoconstructs, trastuzumab delivery, two-step targeting

Received: September 29, 2017
Revised: November 20, 2017
Published online: January 8, 2018

[1] a) A. M. Scott, J. D. Wolchok, L. J. Old, *Nat. Rev. Cancer* **2012**, *12*, 278; b) O. H. Brekke, I. Sandlie, *Nat. Rev. Drug Discovery* **2003**, *2*, 52; c) A. Beck, L. Goetsch, C. Dumontet, N. Corvaia, *Nat. Rev. Drug Discovery* **2017**, *16*, 315; d) H. K. Gan, M. van den Bent, A. B. Lassman, D. A. Reardon, A. M. Scott, *Nat. Rev. Clin. Oncol.* **2017**, *14*, 695.

[2] a) D. Gajria, S. Chandarlapaty, *Expert Rev. Anticancer Ther.* **2011**, *11*, 263; b) D. Slamon, W. Eiermann, N. Robert, T. Pienkowski, M. Martin, M. Press, J. Mackey, J. Glaspy, A. Chan, M. Pawlicki, T. Pinter, V. Valero, M.-C. Liu, G. Sauter, G. von Minckwitz, F. Visco, V. Bee, M. Buyse, B. Bendahmane, I. Tabah-Fisch, M.-A. Lindsay, A. Riva, J. Crown, G. The Breast Cancer International Research, *N. Engl. J. Med.* **2011**, *365*, 1273; c) C. L. Vogel, M. A. Cobleigh, D. Tripathy, J. C. Gutheil, L. N. Harris, L. Fehrenbacher, D. J. Slamon, M. Murphy, W. F. Novotny, M. Burchmore, S. Shak, S. J. Stewart, M. Press, *J. Clin. Oncol.* **2002**, *20*, 719.

[3] a) N. U. Lin, L. Amiri-Kordestani, D. Palmieri, D. J. Liewehr, P. S. Steeg, *Clin. Cancer Res.* **2013**, *19*, 6404; b) J. P. Leone, B. A. Leone, *Exp. Hematol. Oncol.* **2015**, *4*, 33; c) A. M. Brufsky, M. Mayer, H. S. Rugo, P. A. Kaufman, E. Tan-Chiu, D. Tripathy, I. C. Tudor, L. I. Wang, M. G. Brammer, M. Shing, M. U. Yood, D. A. Yardley, *Clin. Cancer Res.* **2011**, *17*, 4834.

[4] a) S. A. Chikarmane, S. H. Tirumani, S. A. Howard, J. P. Jagannathan, P. J. DiPiro, *Clin. Radiol.* **2015**, *70*, 1; b) I. Witzel, L. Oliveira-Ferrer, K. Pantel, V. Muller, H. Wikman, *Breast Cancer Res.* **2016**, *18*, 8; c) E. Lim, N. U. Lin, *Oncology* **2014**, *28*, 572; d) M. R. Quigley, O. Fukui, B. Chew, S. Bhatia, S. Karlovits, *Neurosurg. Rev.* **2013**, *36*, 377; e) D. Palmieri, J. L. Bronder, J. M. Herring, T. Yoneda, R. J. Weil, A. M. Stark, R. Kurek, E. Vega-Valle, L. Feigenbaum, D. Halverson, A. O. Vortmeyer, S. M. Steinberg, K. Aldape, P. S. Steeg, *Cancer Res.* **2007**, *67*, 4190; f) H. Kennecke, R. Yerushalmi, R. Woods, M. C. Cheang, D. Voduc, C. H. Speers, T. O. Nielsen, K. Gelmon, *J. Clin. Oncol.* **2010**, *28*, 3271.

[5] a) Y. J. Yu, R. J. Watts, *Neurotherapeutics.* **2013**, *10*, 459; b) S. M. Paul, *Sci. Transl. Med.* **2011**, *3*, 84ps20; c) V. Neves, F. Aires-da-Silva, S. Corte-Real, M. A. R. B. Castanho, *Trends Biotechnol.* **2016**, *34*, 36; d) D. Stanimirovic, K. Kemmerich, A. S. Haqqani, G. K. Farrington, *Adv. Pharmacol. (San Diego, CA, U. S.)* **2014**, *71*, 301.

[6] a) H. L. Wong, X. Y. Wu, R. Bendayan, *Adv. Drug Delivery Rev.* **2012**, *64*, 686; b) C. Saraiva, C. Praca, R. Ferreira, T. Santos, L. Ferreira, L. Bernardino, *J. Controlled Release* **2016**, *235*, 34; c) W. A. Banks, *Nat. Rev. Drug Discovery* **2016**, *15*, 275.

[7] a) J. A. Loureiro, B. Gomes, M. A. Coelho, M. do Carmo Pereira, S. Rocha, *Nanomedicine (London, U. K.)* **2014**, *9*, 709; b) W. M. Pardridge, *Cold Spring Harbor Protoc.* **2010**, *2010*, 5407; c) Y. Chen, L. Liu, *Adv. Drug Delivery Rev.* **2012**, *64*, 640; d) R. J. Boado, Y. Zhang, Y. Zhang, W. M. Pardridge, *Biotechnol. Bioeng.* **2007**, *96*, 381; e) I. van Rooy, E. Mastrobattista, G. Storm, W. E. Hennink, R. M. Schiffelers, *J. Controlled Release* **2011**, *150*, 30; f) W. M. Pardridge, *J. Cereb. Blood Flow Metab.* **2012**, *32*, 1959; g) T. Lin, P. Zhao, Y. Jiang, Y. Tang, H. Jin, Z. Pan, H. He, V. C. Yang, Y. Huang, *ACS Nano* **2016**, *10*, 9999; h) Z. Chai, X. Hu, X. Wei, C. Zhan, L. Lu, K. Jiang, B. Su, H. Ruan, D. Ran, R. H. Fang, L. Zhang, W. Lu, *J. Controlled Release* **2017**, *264*, 102.


© 2018 WILEY-VCH Verlag GmbH & Co. KGaA, Weinheim

[8] P. R. Lockman, R. K. Mittapalli, K. S. Taskar, V. Rudraraju, B. Gril, K. A. Bohn, C. E. Adkins, A. Roberts, H. R. Thorsheim, J. A. Gaasch, S. Huang, D. Palmieri, P. S. Steeg, Q. R. Smith, *Clin. Cancer Res.* **2010**, *16*, 5664.

[9] a) A. I. Mehta, A. M. Brufsky, J. H. Sampson, *Cancer Treat. Rev.* **2013**, *39*, 261; b) W. M. Pardridge, R. J. Boado, *Methods Enzymol.* **2012**, *503*, 269; c) J. Kreuter, *Adv. Drug Delivery Rev.* **2014**, *71*, 2.

[10] M. Kinoshita, N. McDannold, F. A. Jolesz, K. Hynynen, *Proc. Natl. Acad. Sci. USA* **2006**, *103*, 11719.

[11] a) Y. J. Yu, J. K. Atwal, Y. Zhang, R. K. Tong, K. R. Wildsmith, C. Tan, N. Bien-Ly, M. Hersom, J. A. Maloney, W. J. Meilandt, D. Bumbaca, K. Gadkar, K. Hoyte, W. Luk, Y. Lu, J. A. Ernst, K. Scearce-Levie, J. A. Couch, M. S. Dennis, R. J. Watts, *Sci. Transl. Med.* **2014**, *6*, 261ra154; b) W. M. Pardridge, *Expert Opin. Drug Delivery* **2015**, *12*, 207; c) R. J. Boado, J. Z. Lu, E. K. Hui, H. Lin, W. M. Pardridge, *Mol. Pharm.* **2016**, *13*, 1385; d) J. Niewoehner, B. Bohrmann, L. Collin, E. Urich, H. Sade, P. Maier, P. Rueger, J. O. Stracke, W. Lau, A. C. Tissot, H. Loetscher, A. Ghosh, P. O. Freskgard, *Neuron* **2014**, *81*, 49; e) Y. J. Yu, Y. Zhang, M. Kenrick, K. Hoyte, W. Luk, Y. Lu, J. Atwal, J. M. Elliott, S. Prabhu, R. J. Watts, M. S. Dennis, *Sci. Transl. Med.* **2011**, *3*, 84ra44.

[12] A. Datta-Mannan, J. E. Croy, L. Schirtzinger, S. Torgerson, M. Breyer, V. J. Wroblewski, *mAbs* **2016**, *8*, 969.

[13] F. A. Harding, M. M. Stickler, J. Razo, R. B. DuBridge, *mAbs* **2010**, *2*, 256.

[14] a) N. Shi, Y. Zhang, C. Zhu, R. J. Boado, W. M. Pardridge, *Proc. Natl. Acad. Sci. USA* **2001**, *98*, 12754; b) N. Shi, R. J. Boado, W. M. Pardridge, *Pharm. Res.* **2001**, *18*, 1091; c) H. L. Wong, N. Chattopadhyay, X. Y. Wu, R. Bendayan, *Adv. Drug Delivery Rev.* **2010**, *62*, 503; d) I. Khalin, R. Alyautdin, T. W. Wong, J. Gnanou, G. Kocherga, J. Kreuter, *Drug Delivery* **2016**, *23*, 3520.

[15] I. Brasnjevic, H. W. Steinbusch, C. Schmitz, P. Martinez-Martinez, *Prog. Neurobiol. (N. Y.)* **2009**, *87*, 212.

[16] a) P. Ramge, R. E. Unger, J. B. Oltrogge, D. Zenker, D. Begley, J. Kreuter, H. Von Briesen, *Eur. J. Neurosci.* **2000**, *12*, 1931; b) J. Kreuter, P. Ramge, V. Petrov, S. Hamm, S. E. Gelperina, B. Engelhardt, R. Alyautdin, H. von Briesen, D. J. Begley, *Pharm. Res.* **2003**, *20*, 409; c) S. Wagner, A. Zensi, S. L. Wien, S. E. Tschickardt, W. Maier, T. Vogel, F. Worek, C. U. Pietrzik, J. Kreuter, H. von Briesen, *PLoS One* **2012**, *7*, e32568; d) P. Blasi, S. Giovagnoli, A. Schoubben, M. Ricci, C. Rossi, *Adv. Drug Delivery Rev.* **2007**, *59*, 454; e) J. Li, P. Cai, A. Shalviri, J. T. Henderson, C. He, W. D. Foltz, P. Prasad, P. M. Brodersen, Y. Chen, R. DaCosta, A. M. Rauth, X. Y. Wu, *ACS Nano* **2014**, *8*, 9925; f) C. He, P. Cai, J. Li, T. Zhang, L. Lin, A. Z. Abbasi, J. T. Henderson, A. M. Rauth, X. Y. Wu, *J. Controlled Release* **2017**, *246*, 98.

[17] K. B. Kurakhmaeva, I. A. Djindjikhashvili, V. E. Petrov, V. U. Balabanyan, T. A. Voronina, S. S. Trofimov, J. Kreuter, S. Gelperina, D. Begley, R. N. Alyautdin, *J. Drug Targeting* **2009**, *17*, 564.

[18] J. A. Couch, Y. J. Yu, Y. Zhang, J. M. Tarrant, R. N. Fuji, W. J. Meilandt, H. Solanoy, R. K. Tong, K. Hoyte, W. Luk, Y. Lu, K. Gadkar, S. Prabhu, B. A. Ordonia, Q. Nguyen, Y. Lin, Z. Lin, M. Balazs, K. Scearce-Levie, J. A. Ernst, M. S. Dennis, R. J. Watts, *Sci. Transl. Med.* **2013**, *5*, 183ra57.

[19] S. Ohshima-Hosoyama, H. A. Simmons, N. Goecks, V. Joers, C. R. Swanson, V. Bondarenko, R. Velotta, K. Brunner, L. D. Wood, R. H. Hruban, M. E. Emborg, *PLoS One* **2012**, *7*, e39036.

[20] a) D. Cardinale, A. Colombo, R. Torrisi, M. T. Sandri, M. Civelli, M. Salvatici, G. Lamantia, N. Colombo, S. Cortinovis, M. A. Dessanai, F. Nole, F. Veglia, C. M. Cipolla, *J. Clin. Oncol.* **2010**, *28*, 3910; b) D. Vucicevic, E. J. Carey, N. J. Karlin, *Breast Care* **2013**, *8*, 146.

[21] a) A. Shalviri, G. Raval, P. Prasad, C. Chan, Q. Liu, H. Heerklotz, A. M. Rauth, X. Y. Wu, *Eur. J. Pharm. Biopharm.* **2012**, *82*, 587; b) A. Shalviri, P. Cai, A. M. Rauth, J. T. Henderson, X. Y. Wu, *Drug Delivery Transl. Res.* **2012**, *2*, 437.

[22] A. W. Vermeer, W. Norde, *Biophys. J.* **2000**, *78*, 394.

[23] a) D. Peer, J. M. Karp, S. Hong, O. C. FaroKHzad, R. Margalit, R. Langer, *Nat. Nanotechnol.* **2007**, *2*, 751; b) A. Albanese, P. S. Tang, W. C. W. Chan, *Annu. Rev. Biomed. Eng.* **2012**, *14*, 1.

[24] A. Shalviri, H. K. Chan, G. Raval, M. J. Abdekhodaie, Q. Liu, H. Heerklotz, X. Y. Wu, *Colloids Surf., B* **2013**, *101*, 405.



© 2018 WILEY-VCH Verlag GmbH & Co. KGaA, Weinheim